Monthly Notices
of the
ROYAL ASTRONOMICAL SOCIETY

MNRAS **501,** 541–547 (2021)
Advance Access publication 2020 October 29

doi:10.1093/mnras/staa3352

A targeted search for repeating fast radio bursts associated with gamma-ray bursts

Nipuni T. Palliyaguru [1,2]★ Devansh Agarwal,[3,4] Golnoosh Golpayegani,[3,4,5] Ryan Lynch,[6,7] Duncan R. Lorimer,[3,4]★ Benjamin Nguyen,[8] Alessandra Corsi[1] and Sarah Burke-Spolaor[3,4,9]

[1]*Department of Physics and Astronomy, Texas Tech University, Lubbock, TX 79409-1051, USA*
[2]*Arecibo Observatory, HC3 Box 53995, Arecibo, PR 00612, Puerto Rico*
[3]*Department of Physics and Astronomy, West Virginia University, Morgantown, WV 26506-6315, USA*
[4]*Center for Gravitational Waves and Cosmology, West Virginia University, Chestnut Ridge Research Building, Morgantown, WV 26505, USA*
[5]*Department of Astronomy, University of California, Berkeley, 501 Campbell Hall #3411, Berkeley, CA 94720, USA*
[6]*Green Bank Observatory, PO Box 2, Green Bank, WV 24944, USA*
[7]*National Radio Astronomy Observatory, Charlottesville, VA 22903, USA*
[8]*Department of Physics and Astronomy, Franklin and Marshall College, Lancaster, PA 17604, USA*
[9]*CIFAR Azrieli Global Scholars, CIFAR, Toronto, ON M5G 1M1, Canada*

Accepted 2020 October 21. Received 2020 September 30; in original form 2020 July 26

ABSTRACT

The origin of fast radio bursts (FRBs) still remains a mystery, even with the increased number of discoveries in the last 3 yr. Growing evidence suggests that some FRBs may originate from magnetars. Large, single-dish telescopes such as Arecibo Observatory (AO) and Green Bank Telescope (GBT) have the sensitivity to detect FRB 121102-like bursts at gigaparsec distances. Here, we present searches using AO and GBT that aimed to find potential radio bursts at 11 sites of past gamma-ray bursts that show evidence for the birth of a magnetar. We also performed a search towards GW170817, which has a merger remnant whose nature remains uncertain. We place 10σ fluence upper limits of $\approx$0.036 Jy ms at 1.4 GHz and $\approx$0.063 Jy ms at 4.5 GHz for the AO data and fluence upper limits of $\approx$0.085 Jy ms at 1.4 GHz and $\approx$0.098 Jy ms at 1.9 GHz for the GBT data, for a maximum pulse width of $\approx$42 ms. The AO observations had sufficient sensitivity to detect any FRB of similar luminosity to the one recently detected from the Galactic magnetar SGR 1935+2154. Assuming a Schechter function for the luminosity function of FRBs, we find that our non-detections favour a steep power-law index ($\alpha \lesssim -1.1$) and a large cut-off luminosity ($L_0 \gtrsim 10^{41}$ erg s^{-1}).

Key words: fast radio bursts – gamma-ray bursts – radio continuum: transients.

1 INTRODUCTION

Fast radio bursts (FRBs; Lorimer et al. 2007; Thornton et al. 2013) are millisecond-duration radio pulses with large dispersion measures (DM), generally known to be of cosmological origin [for recent reviews, see Petroff, Hessels & Lorimer (2019) and Cordes & Chatterjee (2019)], with the exception of FRBs from the Galactic magnetar SGR 1935+2154 (Bochenek et al. 2020; CHIME/FRB collaboration 2020). Measurements to date imply total isotropic energies of the order of $\approx 10^{38}$–10^{40} erg (Dolag et al. 2015; Law et al. 2017; Zhang 2018), and high brightness temperatures that point to coherent emission processes. So far, there are over 100 known FRBs[1] (Petroff et al. 2016) with $\approx$20 repeating (Spitler et al. 2016; CHIME/FRB Collaboration 2019a, b; Fonseca et al. 2020). Over 50 were found within the last 3 yr by The Australian Square Kilometre Array Pathfinder (Shannon et al. 2018) and The Canadian Hydrogen Intensity Mapping Experiment (CHIME; CHIME/FRB Collaboration 2018).

Despite this rapid growth in observational results, the origin of FRBs is still uncertain. Theories proposed to explain the origin of FRBs include giant flares from magnetars (Popov & Postnov 2010; Kulkarni et al. 2014; Metzger, Berger & Margalit 2017), giant pulses powered by spin-down from extragalactic neutron stars (NSs; Cordes & Wasserman 2016), produced from infalling asteroids to the pulsar's magnetosphere (Dai et al. 2016), collapse of massive NSs (Falcke & Rezzolla 2014), or compact binary mergers. While there may be multiple classes of FRBs (Palaniswamy, Li & Zhang 2018), the repeaters rule out catastrophic progenitors, at least for those particular objects. The localization of the repeating FRB 121102 (Spitler et al. 2016) to a low-metallicity dwarf galaxy (Chatterjee et al. 2017; Tendulkar et al. 2017) started pointing to a NS origin for FRBs. The more recent discovery of FRBs from the Galactic source SGR 1935+2154 (Bochenek et al. 2020; CHIME/FRB collaboration 2020) further confirms this. The idea of a millisecond magnetar, a NS with millisecond birth period and a large magnetic field ($>10^{15}$ G), being responsible for the FRBs has been put forward since the discovery of FRBs (Popov & Postnov 2010) and recently invoked to explain FRB121102 (Metzger et al. 2017). Connections have also been made previously between FRBs and soft gamma repeaters (SGRs), where the sudden release in magnetic energy that powers the SGR may also produce an FRB (Katz 2016; Bochenek et al. 2020; CHIME/FRB collaboration 2020). In SGRs, magnetic

★ E-mail: npalliya@mix.wvu.edu (NTP); Duncan.Lorimer@mail.wvu.edu (DRL)
[1]http://frbcat.org

reconnection produces a strong magnetic pulse that propagates outwards and interacts with the surrounding gas, which could power a millisecond-duration burst in the radio band (Lyubarsky 2014).

Millisecond magnetars may be born in the core collapse of massive stars and/or in the merger of binary NSs (e.g. Usov 1992; Dai & Lu 1998). The rotational energy of a NS is given by

$$E_{\rm rot} \approx 2 \times 10^{52}\,{\rm erg} \left(\frac{M}{1.4\,{\rm M}_{\odot}}\right) \left(\frac{R}{10\,{\rm km}}\right)^{2} \left(\frac{P}{1\,{\rm ms}}\right)^{-1}. \quad (1)$$

Rapid rotation (periods of milliseconds) gives sufficient rotational energy to power a gamma-ray burst (GRB; Metzger et al. 2011). Therefore, GRBs with intrinsic energy $<10^{52}$ erg (which is the maximum rotational energy) may be powered by magnetars. Energy injection from a rapidly rotating magnetar is often invoked to explain the energy in GRBs with a supernova (SN) connection (hereafter, called GRB-SNe; Mazzali et al. 2014). By comparing the kinetic energy of the associated SN and the gamma-ray energy, Mazzali et al. (2014) show that a magnetar central engine likely powers all GRB-SNe. In this scenario, the spin-down energy of a highly magnetized NS is deposited in the ejecta.

Evidence for the formation of NSs is also seen in some GRBs as a shallower-than-normal decay in the X-ray light curves (Zhang & Mészáros 2001; Corsi & Mészáros 2009). For some of these GRBs, the central engine could be a magnetar, which did not immediately collapse to a black hole (BH), where the spin-down energy is deposited into the ejecta, giving rise to X-ray plateaus (Rowlinson et al. 2013).

A merger that produces a stable NS that is rotationally supported may also quite possibly be a source of repetitive FRBs (Yamasaki et al. 2018). The general picture concerning binary neutron star (BNS) mergers is that the merger produces either a BH or a long-lived NS depending on the equation of state (EOS) and the maximum allowable mass for a NS, $M_{\rm max}$, which could be more than 2.1 $M_{\odot}$ (Cromartie et al. 2020). For BNS total mass of $\approx$1.3–1.6$M_{\rm max}$, prompt collapse to a BH occurs, for masses $\lesssim$1.2$M_{\rm max}$, a hypermassive NS is formed as an intermediate product, which then loses angular momentum and collapses to a BH (Margalit & Metzger 2017), and for low-mass BNS, an indefinitely long-lived NS may be formed (Margalit & Metzger 2017).

The FRB–GRB connection has also been discussed previously, with FRBs resulting from the collapse of a supra-massive NS to a BH (Zhang 2014). Palaniswamy et al. (2014) searched for prompt radio emission coincident with GRBs, but these searches could have suffered from low sensitivity (system equivalent flux density (SEFD) >800 Jy), whereas a typical FRB would have a flux density of $\approx$0.5 Jy. Several other campaigns that followed up GRBs in search of FRBs have yielded non-detections (Madison et al. 2019; Men et al. 2019; Hilmarsson et al. 2020). However, Bannister et al. (2012) detected candidate single pulses from GRBs, DeLaunay et al. (2016) identified a gamma-ray transient in connection with an FRB, whose high isotropic gamma-ray energy may be attributed to a magnetar origin, and Wang et al. (2020) identified a marginal association between FRB 171209 and GRB 110715A. Adding to these, the presence of an SN remnant is one explanation for the large rotation measure (RM) and the highly magnetized environment of the FRB121102 (Michilli et al. 2018). Intriguingly, Nicholl et al. (2017) found that FRBs arising predominantly from repetitive sources, i.e. originating from magnetars, occur at a rate of $10^4\,{\rm Gpc}^{-3}$, consistent with the rates derived from observations. It is also worthwhile pointing out that the birth rate of non-repeating FRBs ($\sim$2700 $\rm yr^{-1}\,Gpc^{-3}$) is consistent with the high end of the BNS merger rate (Nicholl et al. 2017; Yamasaki et al. 2017).

Motivated by these ideas, we targeted several relatively nearby GRB sites and the BNS merger GW170817 in search of possible FRB signals. A sensitive telescope like Arecibo should be able to detect FRB121102-like bursts of flux density 1.8 mJy (Palaniswamy et al. 2014) to a distance of up to $\approx$4.8 Gpc. The details of our FRB search observations are presented in Section 2 and data analysis is presented in Section 3. We present results and place constraints on FRB progenitors in Section 4, and we offer our conclusions in Section 5.

2 OBSERVATIONS

Our target list contains 11 GRBs visible in the Arecibo Observatory (AO) declination range and the BNS merger GW 170817, which was observed with the Green Bank Telescope (GBT). Out of the 11 GRBs, there are six long GRBs (lGRBs) with SN associations, and five GRBs (one lGRB and four short GRBs; sGRBs) that exhibit plateaus in the X-ray light curve. The target list and their properties are given in Table 1. All GRBs have been localized to a region <2.5 arcsec by high-energy observations, which allows single-dish telescopes with a field of view (FoV) of a few arcminutes to cover the entire localization error region at full sensitivity.

Full stokes (or polarization self-and cross-products), 8-bit, high time resolution spectra were recorded at both telescopes. A known pulsar was observed at the start of each observation session to verify the status of instruments. Table 2 lists information about the observational set-up for AO and GBT. The dates since the GRB trigger, on which the observations were conducted, are shown in Fig. 1. The total and average observation time duration of each GRB is listed in Table 3.

Arecibo observations were carried out between 2017 December 12:50 UTC and 2018 December 19:55 UTC. Arecibo targets were observed for $\sim$0.6 h on each epoch. A total of 114 h of observations were obtained on all GRBs, with 1–21 h on each target at each frequency depending on the local sidereal time (LST) availability. We note that all of the sources are away from the Galactic plane. Data were recorded using the Puerto Rico Ultimate Pulsar Processing Instrument (PUPPI) at centre frequencies of 1380 MHz and 4.5 GHz with a bandwidth of $\approx$600 MHz with 512 frequency channels and sampled at 40.96 µs.

GBT observations were carried out between 2017 November 02:41 UTC and 2018 July 31:02 UTC on 10 epochs. GW 170817 was observed for $\sim$1 h at each frequency during each observation. Since low-frequency emission may be self-absorbed by the post-GRB ejecta at early epochs, observations were conducted at 1.4 and 1.9 GHz on the first two epochs and afterwards only at 1.4 GHz on the following epochs. The GBT data were recorded on the Green Bank Ultimate Pulsar Processing Instrument (GUPPI) spectrometer with a sampling time of 10.24 µs. To minimize any intrachannel dispersive smearing to that caused by the difference between the true and estimated DM, data were semicoherently de-dispersed at a DM of 80 $\rm cm^{-3}$ pc. This DM is an estimate corresponding to DM = $\rm DM_{MW}$ + $\rm DM_{IGM}$ + $\rm DM_{H}$, where $\rm DM_{MW} = 35\,cm^{-3}$ pc is the contribution from the Milky Way (Yao, Manchester & Wang 2017), $\rm DM_{IGM} = 7\,cm^{-3}$ pc is the intergalactic medium (Ioka 2003), and $\rm DM_{H} = 35\,cm^{-3}$ pc is the host galaxy (assuming a host like the Milky Way (MW)). We use $\rm DM_{H} = 35\ cm^{-3}$ pc, which is the approximate DM contribution from the MW for a line of sight out of the plane.

Table 1. The list of targets. Name, redshift, distance, RA, Dec., galactic coordinates (l and b), expected DM, GRB duration (T_{90}), and the minimum detectable luminosity ($L_{\rm min}$) corresponding to S/N = 10 at 1.4 GHz.

Name	Redshift	Distance Mpc	RA (deg)	Dec. (deg)	l (deg)	b (deg)	Expected DM ($\rm cm^{-3}$ pc)	Duration (sec)	$L_{\rm min}$ erg $\rm s^{-1}$
GRB 030329/SN2003dh	0.169	812	10:44:50.03	21:31:18.15	216.98	60.69	264.32	25	1.72×10^{40}
GRB 060218/SN2006aj	0.033	145	03:21:39.69	16:52:01.6	166.92	− 32.88	173.08	2100	5.5×10^{38}
GRB 120422A/SN2012bz	0.280	1434	09:07:38.42	14:01:06.0	215.22	36.437	413.64	5.35	5.38×10^{40}
GRB 130427A/SN2013cq	0.340	1795	11:32:32.63	27:41:51.7	206.51	72.50	472.37	162.83	8.44×10^{40}
GRB 130702A/SN2013dx	0.145	687	14:29:14.78	15:46:26.1	11.35	64.63	241.17	59	1.23×10^{40}
GRB 130215A/SN2013ez	0.597	3508	02:53:56.6	13:23:13.2	163.07	− 39.76	991.80	65.7	3.22×10^{41}
GRB 130603B	0.356	1894	11:28:48.15	17:04:16.9	236.42	68.42	498.47	0.18	9.39×10^{40}
GRB 140903A	0.351	1863	15:52:03.27	27:36:09.4	44.39	50.12	496.38	0.30	9.09×10^{40}
GRB 051221	0.547	2868	21:54:48.71	16:53:28.2	73.54	− 28.58	786.02	1.4	2.15×10^{41}
GRB 100816A	0.803	4529	23:26:57.62	26:34:43.9	100.44	32.57	1396.40	2.9	5.37×10^{41}
GRB 130831A	0.479	2459	23:54:29.91	29:25:47.6	08.33	− 31.82	663.84	32.5	1.58×10^{41}
GW170817	0.0098	42	13:09:48.089	− 23:22:53.35	308.37	39.29 7	77.27	2.0	1.06×10^{38}

Note. References: Stanek et al. (2003), Cano et al. (2014), Mazzali et al. (2014), D'Elia et al. (2015), Abbott et al. (2017), and https://swift.gsfc.nasa.gov/archive/. https://swift.gsfc.nasa.gov/archive/grb_table/

Table 2. Summary of observational set-up. Telescope name, centre frequency ($f_{\rm c}$), system temperature ($T_{\rm sys}$), telescope gain, bandwidth, the number of channels ($N_{\rm chan}$), sampling time ($t_{\rm samp}$), and the FoV.

Name telescope	$f_{\rm c}$ (MHz)	$T_{\rm sys}$ K	Gain ($\rm K\,Jy^{-1}$)	BW (MHz)	$N_{\rm chan}$	$t_{\rm samp}$ μs	FoV $\rm deg^2$
AO	1.4	≈30	8	600	512	40.96	9.5×10^{-3}
AO	4.5	≈30	4	800	512	40.96	7.8×10^{-4}
GBT	1.4	≈20	2.0	800	512	10.24	1.8×10^{-2}
GBT	1.9	≈22	1.9	800	512	10.24	8.7×10^{-3}

Note. $T_{\rm sys}$, gain, and FoV values for AO and GBT are obtained from http://www.naic.edu/~astro/RXstatus/rcvrtabz.shtml and https://science.nrao.edu/facilities/gbt/proposing/GBTpg.pdf, respectively.

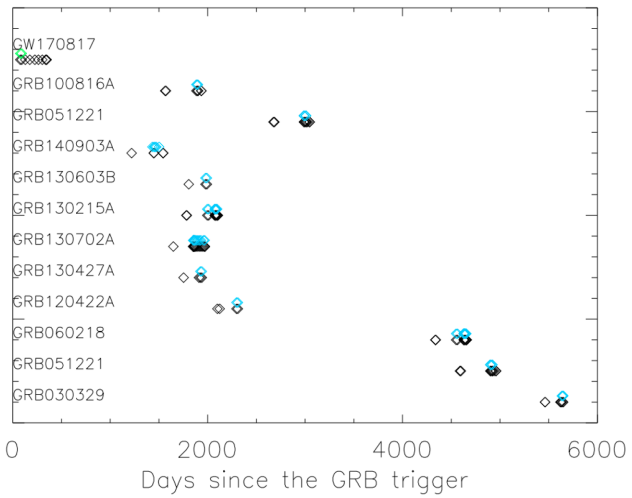

Figure 1. The time-scale of our radio observations for the sources that are listed in Table 1 since the GRB trigger. All observations were made within a time span of 412 d, between the dates of 2017 November 2 and 2018 December 19. Our targets are arbitrarily offset along the y-axis for clarity. Black, blue, and green diamonds represent 1.4, 4.5, and 2 GHz observations, respectively. GRB 130702A was monitored ∼once a month in order to verify the origin of an excess dispersion measure seen on the first observation.

Table 3. GRB name, frequency, total time on the source, the number of epochs observed, and the average time duration of each observation.

Name	Frequency (MHz)	Total time (h)	Number	Average time (h)
GRB 030329	1380	4.5	7	0.65
	4500	1.7	4	0.42
GRB 051221	1380	14.7	15	0.98
	4500	2.5	5	0.51
GRB 060218	1380	8.7	16	0.55
	4500	6.9	13	0.53
GRB 120422A	1380	3.5	4	0.88
	4500	1.2	2	0.60
GRB 130427A	1380	2.7	4	0.67
	4500	1.0	2	0.51
GRB 130702A	1380	13.7	21	0.65
	4500	6.9	15	0.46
GRB 130215A	1380	12.1	19	0.64
	4500	7.5	12	0.63
GRB 130603B	1380	2.3	3	0.76
	4500	1.0	2	0.50
GRB 140903A	1380	4.1	6	0.68
	4500	3.1	6	0.51
GRB 051221	1380	14.7	15	0.98
	4500	2.5	5	0.51
GRB 100816A	1380	5.4	8	0.67
	4500	1.3	3	0.44
GW 170817	1399	8.7	10	0.86
	1999	1.8	2	0.91

3 DATA ANALYSIS

Data from both telescopes were processed with the GPU accelerated pipeline HEIMDALL[2] and the PRESTO analysis package (Ransom 2001).

We search the data at the recorded frequency and time resolution using a GPU accelerated pipeline HEIMDALL. The data were de-dispersed at 1–7000 pc $\rm cm^{-3}$ and were searched for pulse widths of 40.96 μs–41.93 ms with the increments in the power of two. This

[2]https://sourceforge.net/projects/heimdall-astro/

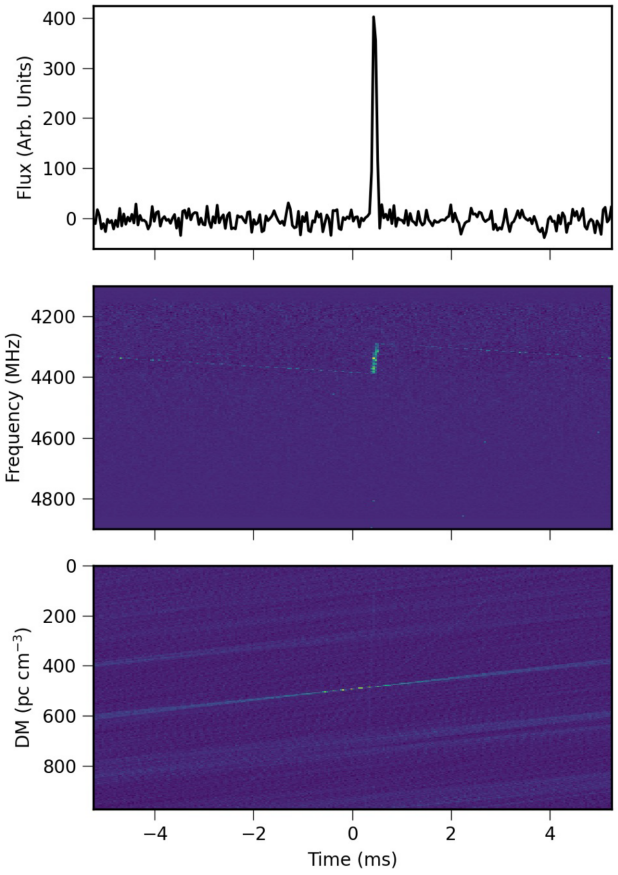

Figure 2. Candidate burst (chirped RFI) from the single-pulse search pipeline in FETCH from GRB 051221 with the brightest signal at DM = 486.4 pc cm^{-3}. The signal is shown as flux density versus time (top), frequency versus time (middle), and DM versus time (bottom).

generated 17 672 candidates above S/N of 6. These candidates were then fed to convolutional neural network Fast Extragalactic Transient Candidate Hunter (FETCH)[3] to classify candidates between radio frequency interference (RFI) and potential FRB candidates (Agarwal et al. 2020). We use model A with a probability threshold of 0.5 for the candidate classification. FETCH labelled 425 candidates as positives. These were inspected manually; 68 candidates were single pulses from the above-mentioned test pulsars. The rest of the candidates were false positives due to a nearby airport radar. Fig. 2 shows an example candidate appearing at a non-zero DM, due to chirped RFI from radar at 4.5 GHz. The appearance of the signal within a narrow band of 4250–4350 MHz confirms the non-astrophysical nature of the signal.

Within PRESTO, RFI excision was done using the tool `rfifind`, which creates a mask in which the affected frequency channels and time chunks are replaced by median values. The data were referenced to the Solar system barycentre and de-dispersed at 1000 trial DMs ranging from 0 to 1000 cm^{-3} pc. For GRB 130215A and GRB 100816A, since the expected DM is >1000 cm^{-3} pc (as listed in Table 1), we search 333 trial DMs ranging from 1000 to 2000 cm^{-3} pc. The dispersion smearing within a channel of $\Delta\nu$ = 800/512 MHz at the lowest frequency of 0.98 GHz from this step size is 8.3 μs DM $\Delta\nu\nu^{-3} \approx 13.7$ μs, which is negligible.

[3]https://github.com/devanshkv/fetch

Significant peaks (>10σ) were searched for, in the de-dispersed time series using the single-pulse pipeline in PRESTO. Each DM versus time plot was visually inspected for real bursts, and those that peaked at a DM of zero were considered as RFI. Candidates that appeared at non-zero DM were reprocessed with `dspsr` (van Straten & Bailes 2011) using the DM and time output by the single-pulse search pipeline in PRESTO, and plotted using PSRCHIVE plotting routines (Hotan, van Straten & Manchester 2004). Candidate bursts detected in the single-pulse search were classified as RFI upon further examination.

4 DISCUSSION

In this section, we discuss the time-scales for radiation to escape the GRB ejecta, the possibility of detecting FRBs from magnetars based on the expected flux density, and the constraints placed on the luminosity function based on non-detections.

4.1 Detectability of a repeating FRB

The environment of the burst/merger site is an important consideration when determining the time-scales for radio emission to escape. The free–free optical depth for the (oxygen-dominated) ejecta would reach $\tau_{\rm eff} = 1$, on a time-scale

$$t = 10 \times \left(93\, f_{\rm ion}^2 \nu_{\rm GHz}^{-2} T_4^{-3/2} M_{10}^2 t_{10} v_9^{-5}\right)^5 \ {\rm yr}, \quad (2)$$

after the explosion (Metzger et al. 2017), where $f_{\rm ion}$ is the ionized fraction of the ejecta, $\nu_{\rm GHz}$ is the observing frequency, M_{10} is the ejectum mass in units of 10 M$_\odot$, and T_4 is the ejectum temperature in units of 10^4 K. Assuming ejectum masses of ∼10 M$_\odot$, $f_{\rm ion}$ = 0.4, ejectum velocities $\sim 10^4$ km s^{-1}, and $T_4 = 1$, radio emission may escape after 6 and 3 yr after the explosion at frequencies of 1 and 4.5 GHz, respectively. With relatively smaller ejectum masses in mergers (than in SNe), ejecta will be transparent to ∼1 GHz emission on a time-scale of several months (Metzger et al. 2017). This could be as soon as ∼3 months for ejectum mass of ∼0.001 M$_\odot$. Our search observations were carried out ≈3 months–15 yr after the explosion.

Measured flux densities of bursts from the repeating FRB 121102 were scaled to the distance of each GRB to estimate the expected flux density if a repeater-like source resided in the GRB site. Assuming radiometer noise limitations for each burst, the signal-to-noise ratio

$$\mathrm{S/N} = \frac{F\, G \sqrt{N_{\rm p} \Delta\nu}}{\beta T_{\rm sys} \sqrt{w}}, \quad (3)$$

where F is the expected fluence given by $F = S\, w$, where S is the flux density, w = 1.0 ms is the pulse width, $T_{\rm sys}$ is the system temperature, G is the telescope gain (the numbers given in Section 2), $\Delta\nu$ is the bandwidth, $\beta = 1.07$ accounts for digitization loss factors, and $N_{\rm p} = 2$ is the number of polarizations (Rane et al. 2016). From the radiometer equation, the minimum flux density corresponding to S/N = 10 for the AO set-up is $S_{\rm min} \approx 36$ mJy at 1.4 GHz and $S_{\rm min} \approx 63$ mJy at 4.5 GHz. The minimum flux density for GBT is $S_{\rm min} \approx 84$ mJy at 1.4 GHz and $S_{\rm min} \approx 98$ mJy at 1.9 GHz. Fig. 3 shows the luminosity distribution and the S/N of 224 bursts at 1.4 and 4–6 GHz from FRB 121102 (Palaniswamy et al. 2014; Hardy et al. 2017; MAGIC Collaboration 2018; Michilli et al. 2018; Spitler et al. 2018; Zhang et al. 2018; Gourdji et al. 2019; Hessels et al. 2019). The S/N histograms for bursts when scaled to the distances of two example GRBs from our sample are also shown at 1.4 and 4.5 GHz. The S/N histograms are created by scaling flux density of FRB 121102 bursts to the distances of the GRBs and calculating the ratio between the expected flux density and minimum flux density

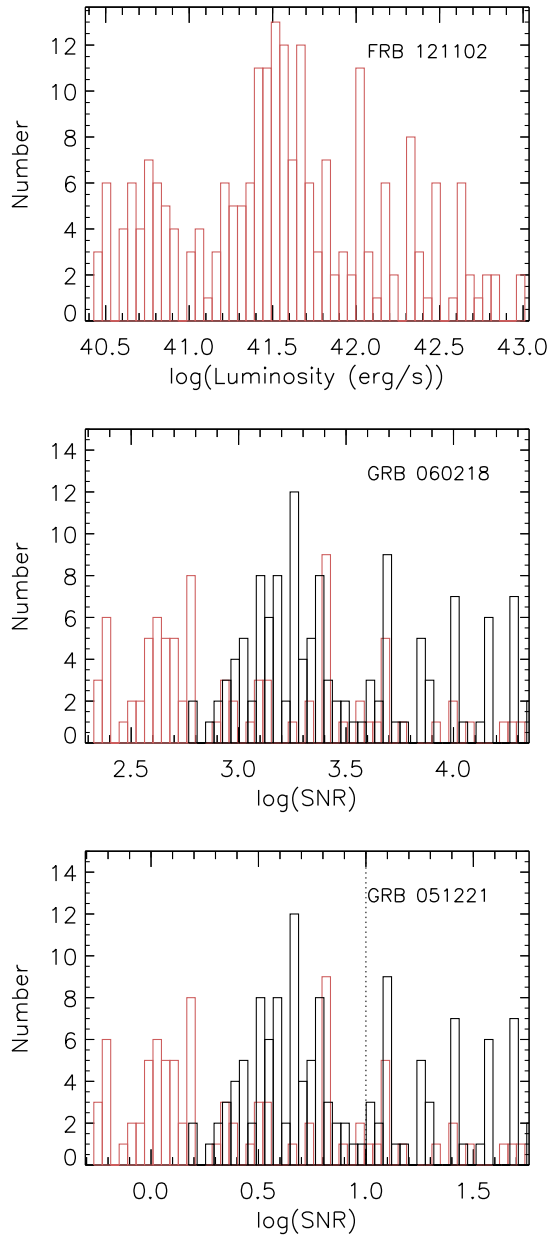

Figure 3. Luminosity distribution of FRB 121102 bursts (top), and S/N histograms of GRB 060218 (middle) and GRB 051221 (bottom). The S/N histograms show the S/N at which FRB 121102-like bursts would be detected at given GRB distances. The black dotted vertical line corresponds to S/N = 10. The red and black S/N histograms represent bursts at 1.4 and 4.5 GHz, respectively.

$S_{\rm min}$. If magnetars emit FRB121102-like bursts, Arecibo should be able to detect the brightest bursts of luminosity $\approx 9 \times 10^{42}$ erg s^{-1} (flux density of 1.8 Jy at 4.5 GHz) at GRB distances of up to 4.8 Gpc.

4.2 Luminosity function

In this section, we attempt to place an upper limit on the FRB rate and constrain the FRB luminosity function parameters based on the non-detection of FRBs in our data. The FRB luminosity function may be expressed by the Schechter function (Schechter 1976) where the event rate density per luminosity interval dL is given by

$$\phi(L)\,{\rm d}L = \phi^*\,(L/L_0)^{\alpha}\,e^{-L/L_0}{\rm d}(L/L_0), \tag{4}$$

where ϕ^* is a reference event rate density, α is the power-law exponent, and L_0 is the cut-off luminosity.

Following Luo et al. (2020), the event rate above a minimum luminosity $L_{\rm min}$ is then given by

$$\begin{aligned} R(>L_{\rm min}) &= \int_{L_{\rm min}/L_0}^{\infty} \phi^*\,(L/L_0)^{\alpha}\,{\rm e}^{(-L/L_0)}{\rm d}\left(\frac{L}{L_0}\right) \\ &= R_0\,\Gamma_i\left(\alpha+1,\frac{L_{\rm min}}{L_0}\right), \end{aligned} \tag{5}$$

where R_0 is the all-sky event rate in sky^{-1} d^{-1} and Γ_i is the incomplete gamma function. Here, we have replaced the volumetric rate by the all-sky rate. The minimum detectable luminosity at the i-th GRB, at a distance D_i, is calculated as $L_{{\rm min},i} = 4\pi\,\Delta\nu\,S_{\rm min}D_i^2$. Here, $\Delta\nu$ is the bandwidth and $S_{\rm min}$ is the minimum detectable flux density, calculated from the radiometer equation. The minimum flux densities corresponding to S/N = 10 for AO and GBT are given in Section 3. Table 1 lists $L_{\rm min}$ values for each GRB at 1.4 GHz. The minimum luminosity of the AO sources at 4.5 GHz is ≈2.3 times larger than at 1.4 GHz. The minimum luminosity for GW 170817 at 1.9 GHz is 1.64×10^{38} erg s^{-1}.

If the i-th GRB site was searched for T_i days, the expected number of pulses for that GRB is

$$n_i = \left(\frac{R\,T_i\,\Omega}{41\,253\,{\rm deg}^2}\right). \tag{6}$$

Here, Ω is the FoV of the telescope (listed in Table 2) and T_i is the observation time on the i-th source. Therefore, assuming a Poisson distribution of pulses, the probability of observing zero pulses in the i-th GRB is $p_i = e^{-n_i}$. The likelihood of not detecting any GRBs in the entire sample, $\mathcal{L}$, is the product of all the probabilities, i.e.

$$\mathcal{L} = \prod_{i=1}^{N} p_i. \tag{7}$$

By summing individual logarithms, we see that

$$\log(\mathcal{L}) = -R_0 \sum_{i=1}^{N} \Gamma_i\left(\alpha+1,\frac{L_{{\rm min},i}}{L_0}\right) T_i \frac{\Omega}{41\,253\,{\rm deg}^2}. \tag{8}$$

For a given non-detection probability, we can place an upper limit on the all-sky rate and place constraints on the parameters of the luminosity function using equation (8). Fig. 4 shows R_0 versus α and L_0 values for 95 per cent probability. We have combined all data from both AO and GBT.

A millisecond magnetar birth rate of ≈170 Gpc^{-3} yr^{-1} and a core-collapse SN rate of $\approx 2.5 \times 10^5$ Gpc^{-3} yr^{-1} (Nicholl et al. 2017), converted to an all-sky rate 0.64 and 937 sky^{-1} d^{-1}, respectively, are marked by the purple region. To convert the volumetric rate to an all-sky rate, we assume that the current AO set-up can detect an FRB of 0.19 mJy at 1.4 GHz (mean flux density of FRB 121102; Palaniswamy et al. 2014) up to a distance of ≈2.2 Gpc with S/N = 10. We also assume a duty cycle of $\eta \approx 0.1$ and a beaming factor of $\xi \approx 0.3$. The sky rate for non-repeating FRBs, scaled to our observations such that $R_0 \approx 1.8 \times 10^4$ sky^{-1} d^{-1} above 36 mJy, is marked by the blue region. Here, we use the expression for the all-sky rate

$$R(>S) = R_0\left(\frac{S}{\rm Jy}\right)^{\alpha'}, \tag{9}$$

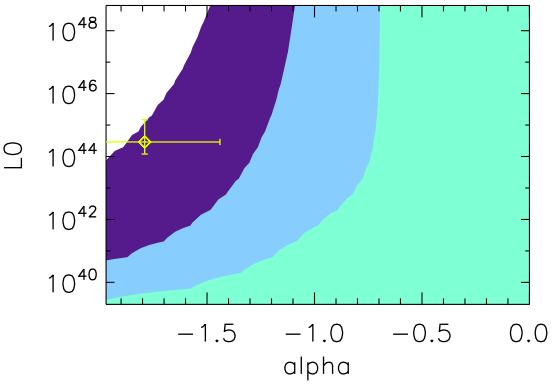

Figure 4. R_0 versus L_0 and α for Schechter function for 95 per cent non-detection probability. The white, purple, light blue, and aqua green regions correspond to $R_0 \lesssim 0.64\,\mathrm{sky^{-1}\,d^{-1}}$, between 0.64 and 937 $\mathrm{sky^{-1}\,d^{-1}}$, between 937 and $1.8 \times 10^4\,\mathrm{sky^{-1}\,d^{-1}}$, and $\gtrsim 1.8 \times 10^4\,\mathrm{sky^{-1}\,d^{-1}}$, respectively. Luo et al. (2020) LF parameters of $L_0 = 2.9^{+11.9}_{-1.7} \times 10^{44}\,\mathrm{erg\,s^{-1}}$ and $\alpha = -1.79^{+0.35}_{-0.31}$ are marked by a yellow diamond.

where S is the minimum flux density, $R_0 = 1140\,\mathrm{sky^{-1}\,d^{-1}}$ is the reference rate at a flux density of 1 Jy, and $\alpha' = -0.83$ is the source count index (Agarwal et al. 2020) from the log N–log S relation (Lawrence et al. 2017). To be consistent with the expected rates of millisecond magnetar formation, L_0 should be higher for smaller α (purple region). In general, $\alpha \lesssim -1.1$ and $L_0 \gtrsim 10^{41}\,\mathrm{erg\,s^{-1}}$.

Luo et al. (2020) find from real FRBs luminosity function parameters $L_0 = 2.9^{+11.9}_{-1.7} \times 10^{44}\,\mathrm{erg\,s^{-1}}$, $\alpha = -1.79^{+0.31}_{-0.35}$ and a volumetric rate of $\phi^* = 339\,\mathrm{Gpc^{-3}\,yr^{-1}}$. This corresponds to an all-sky rate of $R_0 \approx 42.4\,\mathrm{sky^{-1}\,d^{-1}}$ at 1.4 GHz. From equation (8), we find that $L_0 = 2.9 \times 10^{44}\,\mathrm{erg\,s^{-1}}$ and $\alpha = -1.79$ gives $R_0 \approx 2.4\,\mathrm{sky^{-1}\,d^{-1}}$, above a flux density of 36 mJy, which is marked in Fig. 4. A flat spectrum for FRBs is assumed here. We further note that the all-sky FRB rate for repeaters will be a fraction of this rate.

Recent studies have shown that FRB 121102 shows a periodicity and clustering and therefore the burst distribution may be better described by a Weibull distribution than a Poisson distribution (Oppermann, Yu & Pen 2018). However, this may be the effect of a few strongly clustered bursts and the burst distribution may still be Poissonian (Cruces et al. 2020). The non-detection probability for a Weibull distribution is given by (Oppermann et al. 2018)

$$p = \frac{\Gamma(1/k)\,\Gamma_i(1/k, (T_i r\,\Gamma(1+1/k)^k))}{k\Gamma(1+1/k)}, \tag{10}$$

where k is the shape parameter that describes the degree of clustering, r is the burst rate, T_i is the observation time, Γ is the gamma function, and Γ_i is the incomplete gamma function. For $k = 1$, the Weibull distribution becomes a Poisson distribution and for $k < 1$ clustering with small intervals is favoured (Oppermann et al. 2018). Considering a burst rate of $r = 5.7\,\mathrm{d^{-1}}$ (Oppermann et al. 2018) and scaling the rate to the distance of each GRB, and taking the product of probabilities for each GRB, the total non-detection probability for AO observations is 3.9×10^{-6} for a Poisson process. For a Weibull distribution with $k = 0.34$ (Oppermann et al. 2018), the non-detection probability is 1.8×10^{-5}. Here, we ignore GRB 060218, since it has a high rate and hence a very small non-detection probability.

5 CONCLUSION

We conducted a single-pulse search for FRBs from 12 well-localized targets that show evidence for magnetar formation. The target list includes six GRB-SNe, four sGRBs, one lGRB without an SN association, and GW170817, for which the merger remnant is undetermined. These searches were conducted ∼3 months–15 yr after the explosion. We show that large single-dish telescopes are well suited to detect FRBs from such extragalactic targets at Gpc distances. Our searches resulted in candidates that were confirmed to be either RFI or single pulses from the known test pulsars. Our constraints on the FRB luminosity function parameters, based on non-detection, are consistent with published values.

The detection of a late-time FRB signal from a GRB site would undoubtedly be the smoking gun signature of magnetar birth that would have a tremendous scientific impact with vast implications for fundamental physics and cosmology for this decade (Law et al. 2019). New wide-field radio telescopes have more than doubled the number of FRBs over the last 2 yr. However, even with the increased number of bursts in the last 2 yr, mechanisms that produce FRBs remain a mystery. Determining the observing cadence remains one of the main challenges in targeted searches. If FRBs are indeed related to explosive events, a better understanding of the emission process and the environment of the explosion will help determine factors such as time for radiation to escape and thereby an observing cadence for future targeted searches. Novel techniques to catch possible radio bursts from gravitational wave counterparts are emerging (Clancy et al. 2019). Better algorithms that reduce the number of candidates and distinguish between RFI and real transients are also in place. Furthermore, even though radio telescopes with large fields of view are dominating FRB searches, sensitive single-dish telescopes will continue to play a crucial role in follow-up searches at targeted locations.

ACKNOWLEDGEMENTS

NTP thanks Phill Perrillat, Hector Hernandez, and other AO staff for data quality checks, scheduling, and support with observing. We thank Akshaya Rane, Jayanth Chennamangalam, Andrew Seymour, and Scott Ransom for help with observations and data processing issues. The AO is a facility of the National Science Foundation (NSF) operated under cooperative agreement by the University of Central Florida in alliance with Yang Enterprises, Inc. and Universidad Metropolitana. The Green Bank Observatory is a facility of the National Science Foundation operated under cooperative agreement by Associated Universities, Inc. NTP acknowledges support from start-up funds to J.D. Romano from Texas Tech University. AC acknowledges support from NSF Award #1907975. DRL acknowledges support from the NSF awards AAG-1616042, OIA-1458952, and PHY-1430284. SBS acknowledges support from NSF grant AAG-1714897. SBS is a Canadian Institute for Advanced Research (CIFAR) Azrieli Global Scholar in the Gravity and the Extreme Universe programme.

DATA AVAILABILITY

The data underlying this article will be shared on reasonable request to the corresponding author.

REFERENCES

Abbott B. P. et al., 2017, ApJ, 848, L12
Agarwal D., et al., 2020, MNRAS, 497, 352
Agarwal D., Aggarwal K., Burke-Spolaor S., Lorimer D. R., Garver-Daniels N., 2020, MNRAS, 497, 1661

Bannister K. W., Murphy T., Gaensler B. M., Reynolds J. E., 2012, ApJ, 757, 38
Bochenek C. D., McKenna D. L., Belov K. V., Kocz J., Kulkarni S. R., Lamb J., Ravi V., Woody D., 2020, PASP, 132, 034202
Cano Z. et al., 2014, A&A, 568, A19
Chatterjee S. et al., 2017, Nature, 541, 58
CHIME/FRB Collaboration, 2018, ApJ, 863, 48
CHIME/FRB Collaboration, 2019a, Nature, 566, 235
CHIME/FRB Collaboration, 2019b, ApJ, 885, L24
Cordes J. M., Chatterjee S., 2019, ARA&A, 57, 417
Cordes J. M., Wasserman I., 2016, MNRAS, 457, 232
Corsi A., Mészáros P., 2009, ApJ, 702, 1171
Cromartie H. T. et al., 2020, Nat. Astron., 4, 72
Cruces M., et al., 2020, MNRAS, 500, 448
Dai Z. G., Lu T., 1998, A&A, 333, L87
Dai Z. G., Wang J. S., Wu X. F., Huang Y. F., 2016, ApJ, 829, 27
DeLaunay J. J. et al., 2016, ApJ, 832, L1
Dolag K., Gaensler B. M., Beck A. M., Beck M. C., 2015, MNRAS, 451, 4277
D'Elia V. et al., 2015, A&A, 577, A116
Falcke H., Rezzolla L., 2014, A&A, 562, A137
Fonseca E. et al., 2020, ApJ, 891, L6
Gourdji K., Michilli D., Spitler L. G., Hessels J. W. T., Seymour A., Cordes J. M., Chatterjee S., 2019, ApJ, 877, L19
Hardy L. K. et al., 2017, MNRAS, 472, 2800
Hessels J. W. T. et al., 2019, ApJ, 876, L23
Hilmarsson G. H. et al., 2020, MNRAS, 493, 5170
Hotan A. W., van Straten W., Manchester R. N., 2004, PASA, 21, 302
Ioka K., 2003, ApJ, 598, L79
James Clancy , et al., 2019, MNRAS, 489, L75
Katz J. I., 2016, ApJ, 826, 226
Kulkarni S. R., Ofek E. O., Neill J. D., Zheng Z., Juric M., 2014, ApJ, 797, 70
Law C. J. et al., 2017, ApJ, 850, 76
Law C. J. et al., 2019, preprint, (arXiv:1903.04691)
Lawrence E., Vander Wiel S., Law C., Burke S. S., Bower G. C., 2017, AJ, 154, 117
Lorimer D. R., Bailes M., McLaughlin M. A., Narkevic D. J., Crawford F., 2007, Science, 318, 777
Luo R., Men Y., Lee K., Wang W., Lorimer D. R., Zhang B., 2020, MNRAS, 494, 665
Lyubarsky Y., 2014, MNRAS, 442, L9
Madison D. R. et al., 2019, ApJ, 887, 252
MAGIC Collaboration, 2018, MNRAS, 481, 2479
Margalit B., Metzger B. D., 2017, ApJ, 850, L19
Mazzali P. A., McFadyen A. I., Woosley S. E., Pian E., Tanaka M., 2014, MNRAS, 443, 67
Men Y. et al., 2019, MNRAS, 489, 3643
Metzger B. D., Berger E., Margalit B., 2017, ApJ, 841, 14
Metzger B. D., Giannios D., Thompson T. A., Bucciantini N., Quataert E., 2011, MNRAS, 413, 2031
Michilli D. et al., 2018, Nature, 553, 182
Nicholl M., Williams P. K. G., Berger E., Villar V. A., Alexander K. D., Eftekhari T., Metzger B. D., 2017, ApJ, 843, 84
Oppermann N., Yu H.-R., Pen U.-L., 2018, MNRAS, 475, 5109
Palaniswamy D., Li Y., Zhang B., 2018, ApJ, 854, L12
Palaniswamy D., Wayth R. B., Trott C. M., McCallum J. N., Tingay S. J., Reynolds C., 2014, ApJ, 790, 63
Petroff E., Hessels J. W. T., Lorimer D. R., 2019, A&AR, 27, 4
Petroff E. et al., 2016, PASA, 33, e045
Popov S. B., Postnov K. A., 2010, in Harutyunian H.A., Mickaelian A.M., Yerevan Y. T., eds, Evolution of Cosmic Objects through their Physical Activity. Gitutyun Publ. House NAS RA, p. 129, Armenia
Rane A., Lorimer D. R., Bates S. D., McMann N., McLaughlin M. A., Rajwade K., 2016, MNRAS, 455, 2207
Ransom S. M., 2001, PhD thesis
Rowlinson A., O'Brien P. T., Metzger B. D., Tanvir N. R., Levan A. J., 2013, MNRAS, 430, 10
Schechter P. , 1976, ApJ, 203, 297
Shannon R. M. et al., 2018, Nature, 562, 386
Spitler L. G. et al., 2016, Nature, 531, 202
Spitler L. G. et al., 2018, ApJ, 863, 150
Stanek K. Z. et al., 2003, ApJ, 591, L17
Tendulkar S. P. et al., 2017, ApJ, 834, L7
CHIME/FRB Collaboration , 2020, Nature, 587, 54
Thornton D. et al., 2013, Science, 341, 53
Usov V. V., 1992, Nature, 357, 472
van Straten W., Bailes M., 2011, PASA, 28, 1
Wang X.-G., Li L., Yang Y.-P., Luo J.-W., Zhang B., Lin D.-B., Liang E.-W., Qin S.-M., 2020, ApJ, 894, L22
Yamasaki S., Totani T., Kiuchi K., 2018, PASJ, 70, 39
Yao J. M., Manchester R. N., Wang N., 2017, ApJ, 835, 29
Zhang B. , 2018, ApJ, 867, L21
Zhang B., 2014, ApJ, 780, L21
Zhang B., Mészáros P., 2001, ApJ, 552, L35
Zhang Y. G., Gajjar V., Foster G., Siemion A., Cordes J., Law C., Wang Y., 2018, ApJ, 866, 149

This paper has been typeset from a TEX/LATEX file prepared by the author.